Polymer 49 (2008) 3510–3523

Contents lists available at ScienceDirect

Polymer

journal homepage: www.elsevier.com/locate/polymer

# Effect of inorganic nanoparticles on mechanical property, fracture toughness and toughening mechanism of two epoxy systems

Jun Ma [a,*], Mao-Song Mo [b], Xu-Sheng Du [b], Patrick Rosso [b], Klaus Friedrich [c], Hsu-Chiang Kuan [d]

[a] School of Advanced Manufacturing & Mechanical Engineering, and Mawson Institute, University of South Australia, Mawson Lakes, SA 5095, Australia
[b] Centre for Advanced Materials Technology, School of Aerospace, Mechanical and Mechatronic Engineering, The University of Sydney, NSW 2006, Australia
[c] Institute for Composite Materials, The University of Kaiserslautern, 67663 Kaiserslautern, Germany
[d] School of Materials, Far East University, Taiwan, China

ARTICLE INFO

*Article history:*
Received 4 March 2008
Received in revised form 19 May 2008
Accepted 19 May 2008
Available online 5 June 2008

*Keywords:*
Nanocomposite
Silica
Toughening

ABSTRACT

We investigated the effect of silica nanoparticles on the mechanical property and fracture toughness of two epoxy systems cured by Jeffamine D230 (denoted J230) and 4,4′-diaminodiphenyl sulfone (denoted DDS), respectively. Toughening mechanisms were identified by a tailor-loaded compact tension method which quantitatively recorded the deformation of a damage zone in the vicinity of a sub-critically propagated sharp crack tip. 20 wt% silica nanoparticles' fraction provided 40% improvement in Young's modulus for both systems; it improved the toughness of J230-cured epoxy from 0.73 to 1.68 MPa $m^{1/2}$, and for the other system improved from 0.51 to 0.82 MPa $m^{1/2}$. The nanoparticles not only stiffen, strengthen and toughen epoxy, but reduce the effect of flaws on mechanical performance as well. In both systems, nanosilica particle deformation, internal cavitation and interface debonding were not found, different to previous reports. This could be due to the various hardeners used or different identification techniques employed. The toughening mechanisms of the J230-cured nanocomposite were attributed to the formation and development of a thin dilatation zone and nanovoids, both of which were induced, constrained and thwarted by the stress fields of the silica nanoparticles. Regarding 10 wt% silica-toughen epoxy cured by J230, a thicker and shorter dilatation zone was found, where neither nanoparticles nor nanovoids were observed. With regard to the DDS-cured system, much less dilatation and voids were found due to the hardener used, leading to moderately improved toughness.

© 2008 Elsevier Ltd. All rights reserved.

## 1. Introduction

Recently, inorganic layered silicate has arisen intensive interest for compounding with epoxy [1], but the toughening effect is not ideal, because (a) disorderly exfoliated structure is hard to achieve, and as a result, microcracks form between silicate layers under load; and (b) the interface between silicate layers and the epoxy matrix is weak, leading to debonding of the layers when fractured. By contrast, less known is the epoxy toughened by finely dispersed silica nanoparticles [2–5] and even less known is the toughening mechanisms of the material.

In comparison with the nanoparticle surface modification for compounding with polymers [6,7], the sol–gel technique has been proved to be effective for introducing silica nanoparticles into pre-polymers via chemical reaction between matrix and particle surface [8,9]. Friedrich et al. used silica nanoparticles with a diameter of 20–30 nm to toughen and stiffen epoxy simultaneously [2–5]. However, there is no report on the effect of matrix modulus on the mechanical properties, fracture toughness and toughening mechanisms of the silica nanoparticle-toughened epoxy.

A number of toughening mechanisms were proposed to explain the toughening effect of silica nanoparticles. Friedrich et al. analysed that the nanoparticles caused a high deflection of the crack growth and particle matrix debonding was possible. Those nanoparticles enhanced the shear deformation of the matrix and thus influenced the crack propagation due to the formation of nano- and microscale shear bands [2]. Zhang et al. concluded that the nanoparticle-induced dimples are likely to be the major toughening mechanism by causing energy dissipation; the author assumed that the nanoparticles are close enough to be able to construct a three-dimensional network of interphase material around them [3]. Taylor et al. discounted the toughening mechanisms of crack pinning, crack deflection and immobilised polymer; the nanoparticle debonding and subsequent plastic void growth were considered as the toughening mechanisms [5]. These mechanisms, however,

* Corresponding author. Tel.: +61 8 8302 5117; fax: +61 8 8302 3380.
*E-mail address:* jun.ma@unisa.edu.au (J. Ma).
*URL:* http://people.unisa.edu.au/jun.ma

0032-3861/$ – see front matter © 2008 Elsevier Ltd. All rights reserved.
doi:10.1016/j.polymer.2008.05.043

might be speculations as no TEM evidence was presented. The TEM investigations on a damage zone in the vicinity of a crack tip in a sub-critical condition were well-recognized as the most authoritative method for the toughening mechanism identification.

A double-notch four-point bend (DN-4PB) method, firstly applied in polymers by Yee and Sue [10], was always employed to probe the deformation history of thermoplastics and thermosets in the vicinity of a crack tip under a critical stress state. Under four-point bending, one of the two notches propagates through the entire ligament and the other is sub-critically propagated and stopped at a sub-critical condition. Hence, the unbroken notch preserves information about the damage zone generated just prior to unstable crack propagation. This method critically requires two nearly identical notches on one side of the sample. The more identical the two notches, the closer to critical fracture the unbroken notch is. ISO 13586 and ASTM D5045-99 indicate that a sufficiently sharp crack is a prerequisite for fracture toughness measurement. Thus, we believe that such a sharp crack is of the same importance for probing toughening mechanisms. In our experience [11], an instantly propagated crack made by tapping is sufficiently sharp; this kind of crack is able to propagate 3–6 mm for Single Edge-Notched Bending specimen, and the propagated crack depth depends on the tapping force and the materials tapped. However, it is impossible to make two nearly identical sufficiently sharp cracks for a silica nanoparticle-toughened thermoset sample because of the high modulus induced by the nanoparticles. Therefore, we explored a new method named tl-CT (as elaborated in Section 2) to probe thermoset toughening mechanisms, which provides quantitative control over the degree of deformation in the vicinity of a sub-critically propagated crack.

In this research, we will investigate the effect of silica nanoparticles on the mechanical properties, fracture toughness and toughening mechanisms of two epoxy systems. Based on the TEM investigations in the vicinity of the sub-critically propagated crack tip, we will report new toughening mechanisms for the nanosilica-modified thermoset. These mechanisms may be applicable to other inorganic nanoparticle-modified thermosets. The tl-CT method providing a qualitative deformation at the sub-critically propagated crack tip can be used in other thermosetting materials for fracture mechanism identification.

## 2. Experimental section

### 2.1. Materials

Epoxy resin diglycidyl ether of bisphenol A (DGEBA, Araldite-F) with an epoxide equivalent weight 182–196 g/equiv was supplied by Ciba-Geigy, Australia. The spherical silica nanoparticles (Nanopox F400) were supplied as a colloidal sol (40 wt%) in epoxy by Hanse Chemie AG, Germany. Hardener Jeffamine D230 (denoted J230) was kindly provided by Huntsman (Singapore); hardener 4,4′-diaminodiphenyl sulfone (denoted DDS) was purchased from Chriskev Company, Inc., USA.

DGEBA was mechanically mixed with given amounts of the master batch of epoxy/nanosilica at 100 °C for 60 min to produce a series of nanocomposites with 0–20 wt% silica contents. Then the mixtures were blended with the two hardeners by the following procedures, respectively. (1) When the mixtures were cooled down to 50 °C, stoichiometric amounts of the curing agent J230, calculated from the DGEBA and the master batch, were blended with the mixture for 5 min, followed by degassing. Finally it was poured into release agent-coated rubber moulds and cured at 80 °C for 3 h, followed by 12 h at 120 °C. (2) The mixing temperature increased to 130 °C. Calculated from the DGEBA and the master batch, stoichiometric amounts of DDS were blended with the mixture for 10 min, followed by curing at 130 °C for 17 h.

### 2.2. Morphology

Ultrathin sections of ~50 nm in thickness were microtomed with a diamond knife using a Leica Ultracut S microtome at room temperature. Sections were collected on 200-mesh copper grids and examined using a Philips CM200 Transmission Electron Microscope at an accelerating voltage of 200 kV.

### 2.3. Dynamic mechanical analysis

Dynamic mechanical spectra were obtained at a frequency of 1 Hz on a DMA 2980 Dynamic Mechanical Analyzer (TA Instruments, Inc., USA). A single cantilever clamp with a supporting span of 20.00 mm was used. The rectangular specimen with a thickness of 4 mm and width of 12 mm was tightened on the clamp using a torque of 1 Nm. Specimens cured by J230 were scanned from 40 to 120 °C. With regard to epoxy cured by DDS, a range from 50 to 180 °C was chosen. Data were recorded at a sampling rate of 2 s/point.

### 2.4. Mechanical property

Dumbbell tensile samples with a gauge length of 50 mm were made using a silicone rubber mold and both sides were polished by emery paper until all visible marks disappeared. Then the samples were post-cured at 120 °C for 60 min. Tensile tests were performed at a strain rate of 0.5 mm/min at room temperature using an Instron 5567 tensile machine. An Instron extensometer 2630-100 was used to collect accurate displacement data to measure the modulus; Young's moduli were calculated with 0.005–0.2% strain.

### 2.5. Fracture toughness

Single Edge-Notched Bending (SENB) and Compact Tension (CT) are the two common fracture toughness measurements. SENB is more popular, because it saves material without complicated processing; CT takes more material and needs workshop assistance, but it gives more space for crack preparation. The CT specimens in this research were prepared using a rubber mold and pins according to ISO 13586 with a specimen width $W \sim 30$ mm and thickness $B$ 5–6 mm.

The CT samples were cured in the mold and then both sides were polished by emery paper until all visible marks disappeared. A sufficiently sharp crack was introduced to the sample by razor blade tapping. Tapping a razor blade on thermoset specimen initiates two types of cracks: non-propagated or instantly propagated cracks. Only the instantly propagated cracks are sufficiently sharp for fracture toughness test [11]. Six specimens were tested for each set of data with a crosshead speed of 0.5 mm/min. The $K_{1c}$ and $G_{1c}$ values of CT specimens were calculated according to ISO 13586.

### 2.6. Toughening mechanisms

To identify the toughening mechanisms of high modulus thermoset, we explored a new method for creating a sufficiently sharp crack at a sub-critical condition. It includes the following steps: (a) the fracture toughness of the target material was measured first; (b) an instantly propagated crack was made by tapping a new razor blade into a new CT specimen of the material. Given the toughness value and the specimen size measured, we were able to calculate a critical loading to propagate the crack according to ISO 13586; and (c) when the specimen was mounted on an Instron Machine, 80% of the critical loading (such a loading is called sub-critical loading in the text) was applied on the specimen, during which quantitative deformation occurred in the vicinity of the crack tip corresponding to the applied load. The deformation quantity was dependent on

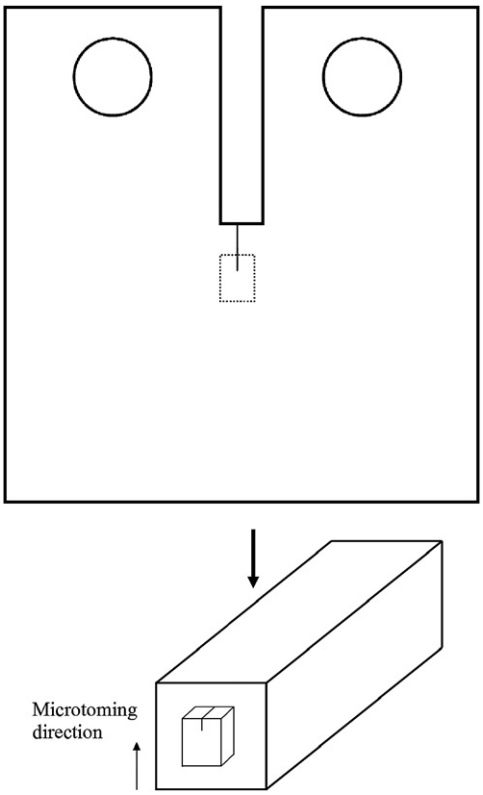


**Fig. 1.** Schematic of TEM sampling process at the crack tip.

the ratio of the applied load to the critical one. Such a crack was at the sub-critical condition for crack propagation. Thus this method using tailor-loaded CT (denoted as tl-CT) provides a damage zone of the naturally sharp crack at a sub-critical condition; the tl-CT preserves information about the damage zone generated just prior to unstable crack propagation. As illustrated in Fig. 1, the block containing the arrested crack tip was cut and glued to an epoxy rod. It was then trimmed to the middle section followed by a rectangular mesa trimming using an optical microscope. Ultrathin sections were carefully cut at 0.1 mm/s with a diamond knife using a Leica Ultracut S microtome at room temperature. As the thin sections containing the deformation zone were fragile, it was transferred to 200-mesh copper grids with great care. To obtain accurate and reproducible microdeformation, 30 sections for each sample were examined using Philips CM200 transmission electron microscope at an accelerating voltage of 200 kV.

The block containing the arrested crack tip was also used for optical microscopic investigation by petrographic polishing [12]. Sections taken from the deformed CT were potted in a room-temperature curing epoxy. These samples were then roughly ground, finely ground, roughly polished, and then finely polished. The polished surface was then mounted onto a clean glass slide using an optically clear epoxy. The sample was allowed to cure overnight at room temperature. Excess material was removed using a bend saw and the sample was again ground and polished until the plane of interest was finally reached. Useful thin sections were ~40 μm thick. All samples were viewed with a Nikon Microscope using crossed-polarized light.

## 3. Results and discussion

### 3.1. Microstructure

Fig. 2 contains typical TEM micrographs of the J230-cured nanocomposite with 20 wt% nanoparticles. At a low magnification (Fig. 2a), the silica nanoparticles are evenly dispersed in the epoxy matrix. Higher magnification image in Fig. 2b shows a mean particle size of 20–30 nm with a narrow range of size distribution, and only little particles with diameter of ~80 nm are found. Different to other polymer/inorganic nanocomposites [13–15] as well as conventional polymer composite [16], these silica nanoparticles show a blurred interface with the matrix (Fig. 2b). Similar conclusion can be obtained for DDS-cured nanocomposite with 20 wt% silica (Fig. 3). These nanoparticles were first synthesized by a sol–gel reaction, then modified by substituting surface silanol groups to functional groups, and finally mixed and reacted with epoxy [8,9]. Further details are unavailable due to confidential commercialization. Numerous studies show that interfacial adhesion provided by the chemical reaction of filler surface functional groups with matrix is critical to nanoparticle dispersion, mechanical properties, damping property and thermal property. Kim et al. reported that the aggregation of silica fillers is highly suppressed in composites filled with epoxide- or amine-modified silica nanoparticles [9]. Given the fine dispersion of the nanoparticles in this study (Figs. 1 and 2), we assume that a strong interface is provided by the chemical reaction of filler surface with matrix. To confirm this, 0.02 g of uncured silica/epoxy was diluted 1000 times with tetrahydrofuran and followed by mechanical mixing for 24 h. Then it was dropped on a carbon film-coated copper grid and observed under TEM. Inorganic silica particles refract electron beam and thus appear dark under TEM; by contrast, carbohydrate cannot refract electron beam and thus appears light. Upon reaction of particle surface with matrix, a layer of carbohydrate is coated on the particle

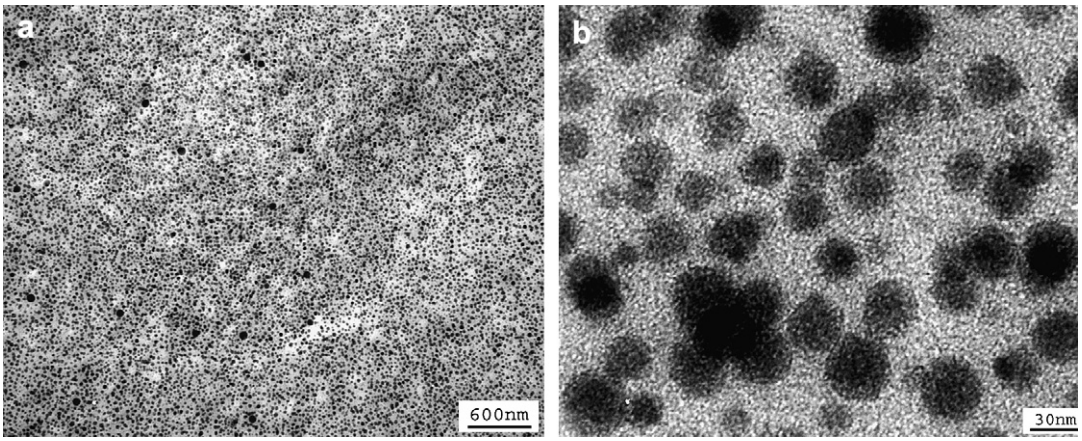


**Fig. 2.** TEM micrographs of J230-cured nanocomposite.

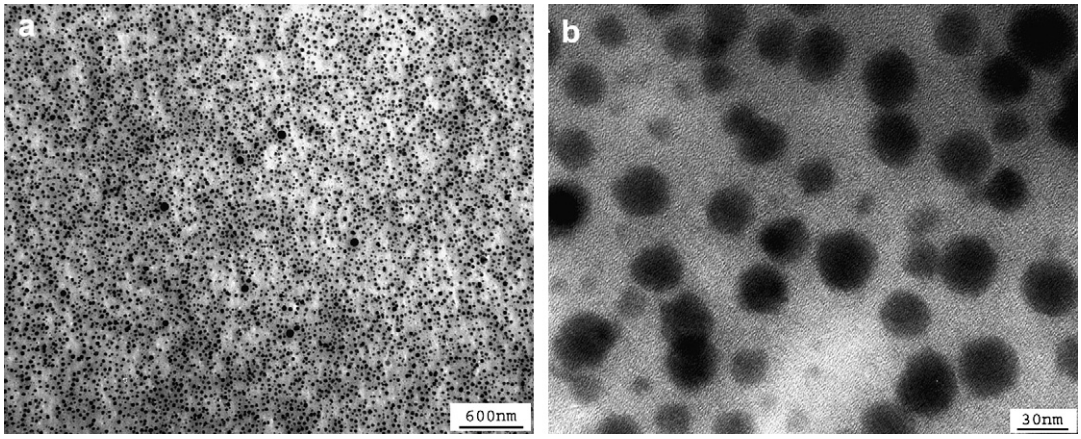


**Fig. 3.** TEM micrographs of DDS-cured nanocomposite.

surface and a layer of light colour is expected under TEM. In Fig. 4, these highly diluted silica nanoparticles demonstrate a distinctive coating material around each particle and this implies a strong interface of the silica nanoparticles used in this research. Damping behaviour of nanocomposite was frequently used to measure the interfacial adhesion of fillers [9]. In Fig. 5a, the magnitude of the tan $\delta$ damping curve of the J230-cured epoxy is significantly reduced throughout the temperature range investigated upon compounding with 20 wt% silica nanoparticles. This suggests that the nanoparticles hinder the energy dissipation process of epoxy molecules. Since the distance between cross-links in this study can be assumed as an epoxy molecule size (about 2–3 nm), these particles may be in motion with the matrix molecules via the grafted chains at a similar time scale and length scale. As a result, the presence of the nanoparticles can hamper the deformation of epoxy, leading to increased glass transition temperature ($T_g$). This result confirms the strong interface of the epoxy/silica nanocomposite. It is supported by Kim's research – nanocomposites with weak interface show essentially no change in $T_g$ and damping with filler contents, while composites with strong interface shown an increase of $T_g$ [9]. Similar conclusion can be obtained for DDS-cured nanocomposite with 20 wt% silica (Fig. 5b). There is no obvious change of damping for both systems toughened by nanosilica. However, an increased damping was reported for epoxy systems toughened by thermoplastics [17,18], which might be due to the incompatibility of microscale particles with epoxy matrixes.

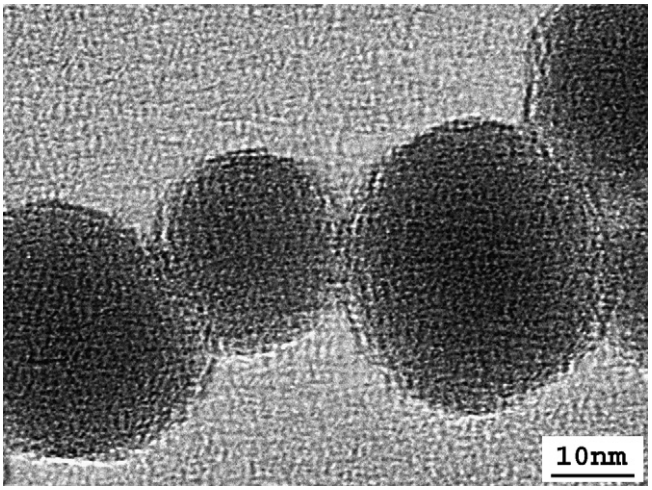


**Fig. 4.** TEM microphotograph of silica/epoxy diluted 1000 times before curing.

### 3.2. Mechanical properties and toughness

The mechanical properties and toughness values of the two epoxy systems toughened by silica nanoparticles were comprehensively listed in Tables 1 and 2.

In Fig. 6, Young's modulus increases significantly with the nanosilica content. The modulus improvement is expected because of the high silica modulus (70 GPa) [19]. Both epoxy systems demonstrate 40% modulus improvement with 20 wt% silica; this indicates that silica nanoparticles can significantly stiffen epoxy, probably independent of the curing agent used.

With increase of the nanoparticle content, the tensile strength of J230-cured epoxy improved slightly, but obvious improvement was found for the DDS-cured epoxy. In the case of epoxy/clay nanocomposite with a better exfoliation, the tensile strength decreased with the addition of clay due to the weak interface between clay and epoxy [20]. By contrast, epoxy/silica nanocomposites demonstrate an increased tensile strength; this confirmed the strong interface between silica nanoparticles and epoxy corresponding to the foregoing DMA and TEM analyses.

It is worth to note the difference of the deviations for tensile strength between neat epoxy and the nanocomposites in Table 2. The large deviation of neat epoxy is caused by impurities or flaws introduced during processing, a well-known fact due to high resin brittleness. The deviation of neat epoxy is significantly reduced by compounding with silica nanoparticles; this implies that silica nanoparticles not only stiffen, strengthen and toughen epoxy, but reduce the effect of flaws on the mechanical performance as well. The reason will be given in toughening mechanism analysis. This conclusion may be useful for the industrial application of epoxy resins.

The tensile stress–strain curves of the two systems are shown in Fig. 7. Silica nanoparticles are able to improve strength and elongation at break simultaneously, leading to an increase of the areas under the curve, this implies toughness enhancement. The J230-cured system displays higher elongation at break than the other system, which is caused by the hardeners used. DDS is a stiff, short molecule. By contrast, J230 molecule is flexible with a repeating unit number of 2–3, leading to a lower crosslink density. Thus, the system cured by J230 demonstrates higher elongation at break.

The effect of silica nanoparticles on the fracture toughness ($K_{1C}$) and the energy release rate ($G_{1C}$) is graphically shown in Fig. 8a–b, respectively. Both $K_{1C}$ and $G_{1C}$ increased significantly with silica fraction: 20 wt% silica significantly enhanced the energy release rate from 0.175 to 0.655 kJ/m$^2$, 274% improvement. Regarding to the system cured by DDS, the toughness improved from 0.073 to 0.132 kJ/m$^2$, 81% improvement.

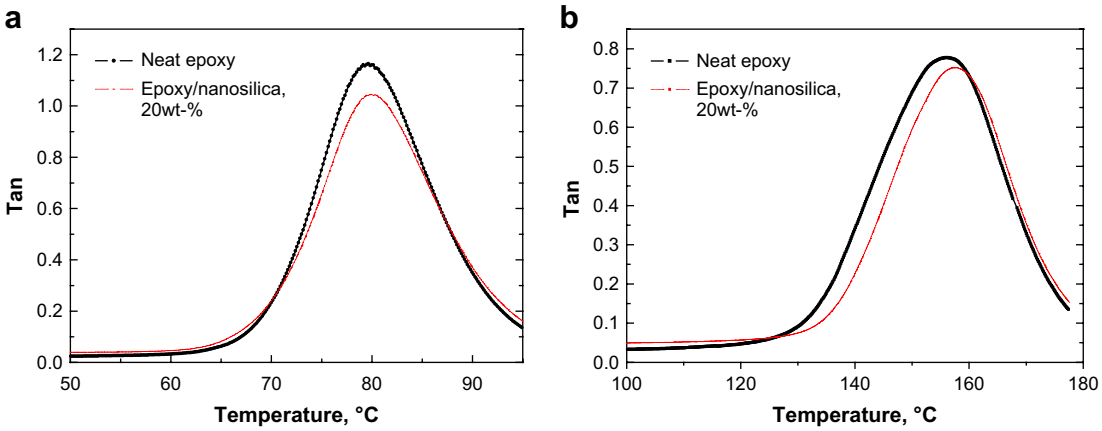


**Fig. 5.** DMA curves of epoxy/silica nanocomposites: (a) cured by J230 and (b) cured by DDS.

**Table 1**
Mechanical properties and toughness of neat epoxy and nanocomposites cured by J230

| Materials | Young's modulus, GPa | Tensile strength, MPa | Plane-strain fracture toughness ($K_{1c}$), MPa m$^{1/2}$ | Critical strain energy release rate[a] ($G_{1c}$), kJ/m$^2$ |
|---|---|---|---|---|
| Neat epoxy | 2.75 ± 0.10 | 57.1 ± 0.5 | 0.73 ± 0.07 | 0.175 ± 0.037 |
| Epoxy/silica nanocomposite, 10 wt% | 3.64 ± 0.17 | 58.3 ± 0.8 | 1.23 ± 0.06 | 0.368 ± 0.039 |
| Epoxy/silica nanocomposite, 20 wt% | 3.85 ± 0.18 | 59.5 ± 0.7 | 1.68 ± 0.07 | 0.655 ± 0.054 |

[a] Calculated according to ISO 13586.

**Table 2**
Mechanical properties and toughness of neat epoxy and nanocomposites cured by DDS

| Materials | Young's modulus, GPa | Tensile strength, MPa | Plane-strain fracture toughness ($K_{1c}$), MPa m$^{1/2}$ | Critical strain energy release rate ($G_{1c}$), kJ/m$^2$ |
|---|---|---|---|---|
| Neat epoxy | 3.20 ± 0.04 | 88.2 ± 14.8 | 0.51 ± 0.04 | 0.073 ± 0.010 |
| Epoxy/silica nanocomposite, 10 wt% | 3.79 ± 0.46 | 104.3 ± 1.5 | 0.69 ± 0.02 | 0.109 ± 0.007 |
| Epoxy/silica nanocomposite, 20 wt% | 4.48 ± 0.24 | 107.4 ± 2.1 | 0.82 ± 0.04 | 0.132 ± 0.014 |

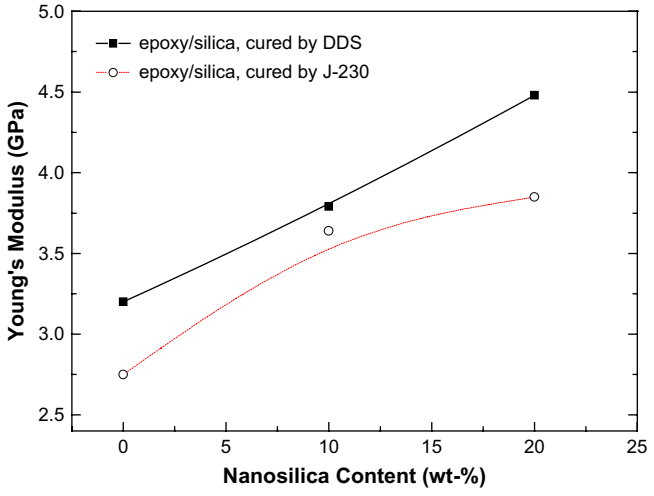


**Fig. 6.** Effect of nanosilica on Young's modulus of the two epoxy systems.

Under a continuous loading condition, the crack propagation in the J230-cured neat epoxy is unstable and exhibits a sawtooth-shaped curve, Fig. 9a, characteristic of the stick-slip mode of crack propagation. Compounding with silica nanoparticles made the crack propagation more unstable, as the load dropped down to zero after propagation. The other system indicates similar trend in Fig. 9b.

### 3.3. Fracture mechanism identification

Fig. 10 shows the optical micrographs of the damage zone in the plane-strain region around the sub-critically propagated crack of J230-cured nanocomposite. When the zone was viewed under crossed polars in Fig. 10b, a small birefringent zone was found, indicating local matrix deformation. In contrast, the nanocomposite cured by DDS reveals smaller birefringent zone in Fig. 11; it means lower degree of local matrix deformation due to the hardener used.

Before identifying the toughening mechanism of the epoxy/silica nanocomposites, it is necessary to clarify the fracture information of neat J230-cured epoxy. Fig. 12a shows a TEM micrograph of the crack tip without loading. An unobvious dilatation zone with 1–2 μm in length was found; this was induced by the crack propagation. Upon a sub-critical loading (see 2.6), the zone developed to ~6 μm in length shown in Fig. 12b, which was obviously caused by the loading. This means that a naturally sharp crack tip of neat J230-cured epoxy is able to create an obvious dilatation zone under loading. Dilatation refers to an expansion in volume of a material under stress, which appears lighter or brighter under TEM. In this case, the dilation zone in Fig. 12a is created by the propagation force of the sharp crack, while the zone in panel b is produced by the sub-critical loading.

Fig. 13 shows TEM micrographs from the vicinity in front of a propagated crack tip of J230-cured nanocomposite containing 20 wt% silica without loading. Different to the neat epoxy (Fig. 12a),

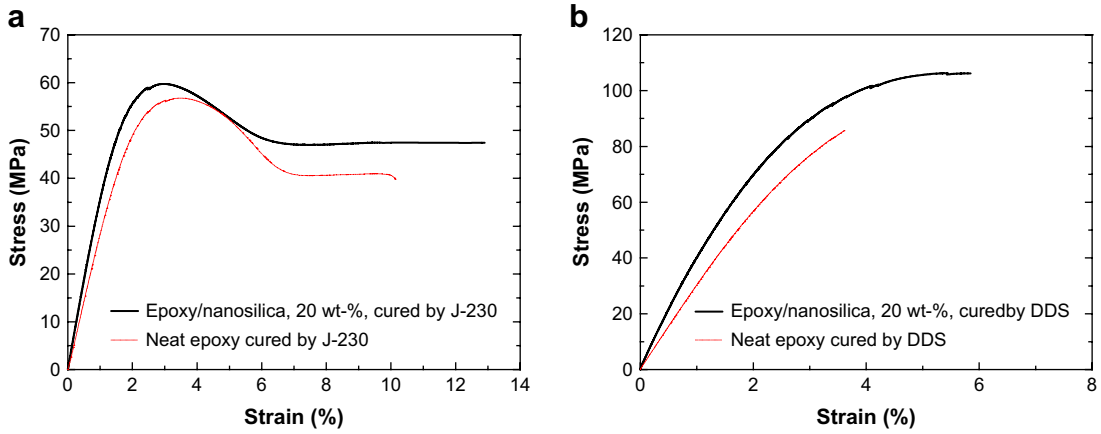


**Fig. 7.** Stress–strain curves of the two epoxy systems: (a) neat epoxy and its nanocomposites cured by J230 and (b) neat epoxy and its nanocomposites cured by DDS.

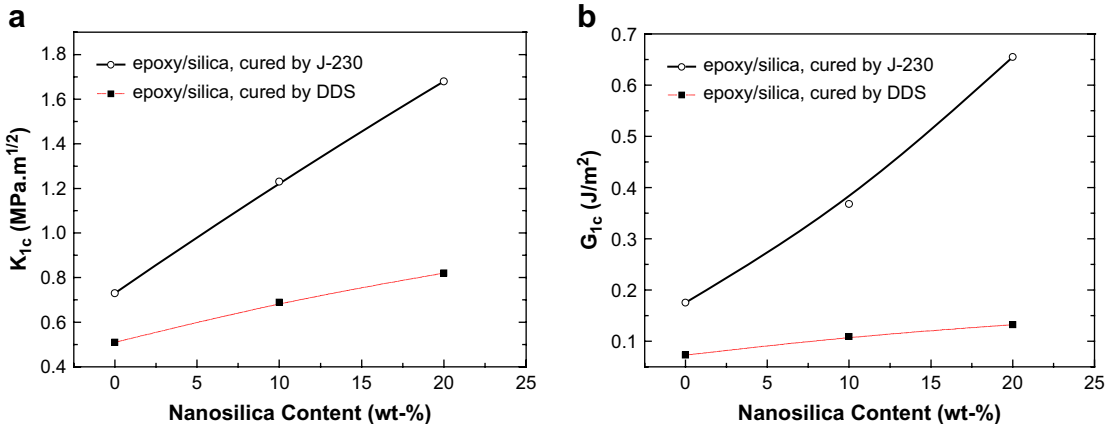


**Fig. 8.** Effect of silica nanoparticles on the fracture toughness of the two epoxy systems: (a) plane-strain fracture toughness and (b) critical strain energy release rate.

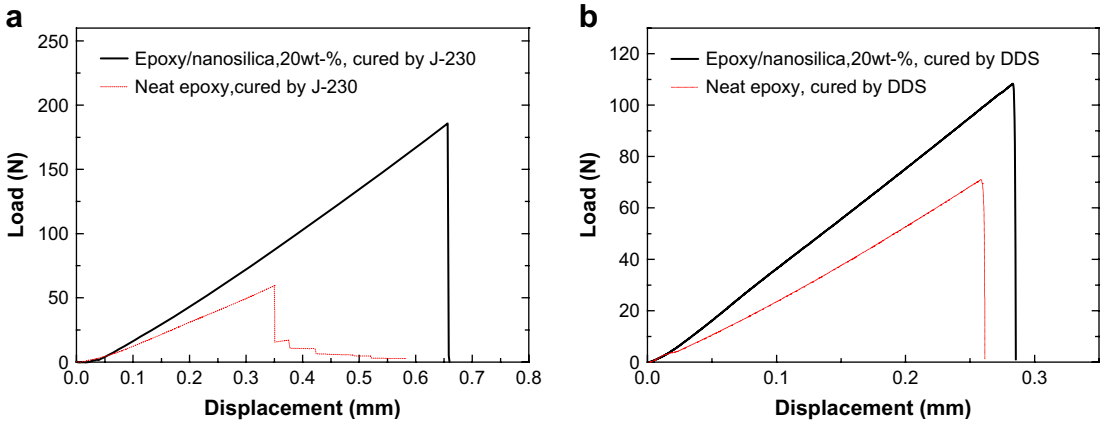


**Fig. 9.** Load–displacement curves of (a) neat epoxy and its nanocomposite cured by J230 and (b) neat epoxy and its nanocomposite cured by DDS.

no dilatation is found in Fig. 13a. A higher magnification (Fig. 13b) displays a lower nanoparticle number per area than the surrounding areas, indicating a lower degree of local dilatation than the neat resin; this is because the silica nanoparticles constrained the matrix deformation. Neither internal particle cavitation nor debonding occurred.

Figs. 14–20 show TEM micrographs from the vicinity in front of the sub-critically propagated crack tip of J230-cured nanocomposite containing 20 wt% silica under a sub-critical loading; these images were taken at different locations along the crack propagation trajectory. A thin dilatation zone of ~100 nm in thickness can be clearly identified in these figures; it extended in the direction of the crack propagation. The formation of this zone must be caused by the toughener phase and/or the intrinsic property (such as modulus) of the matrix, as such a zone was not found for the neat epoxy (Fig. 12b). Higher magnification images in these

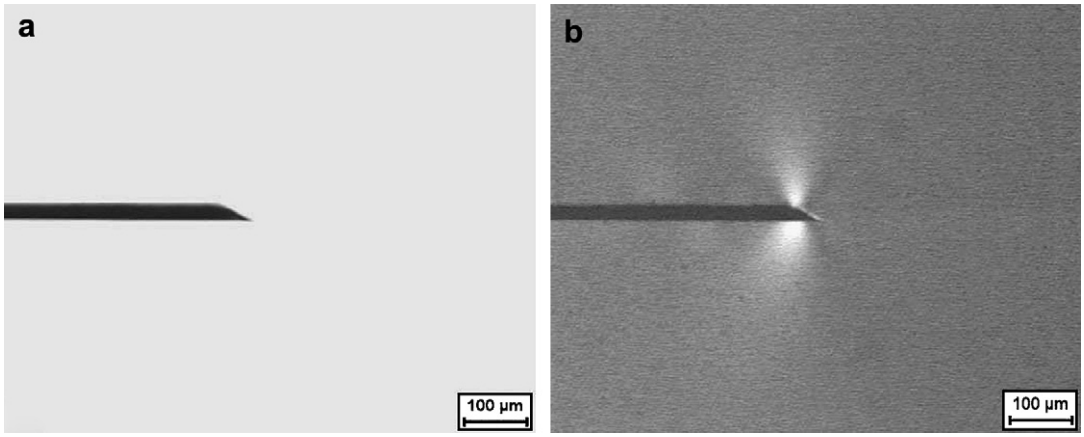


**Fig. 10.** Transmitted light optical micrographs of a section with 30–40 μm in thickness taken at the sub-critically propagated crack in epoxy/nanosilica system cured by J230: (a) under bright field and (b) under crossed polars. The crack propagated from left to right.

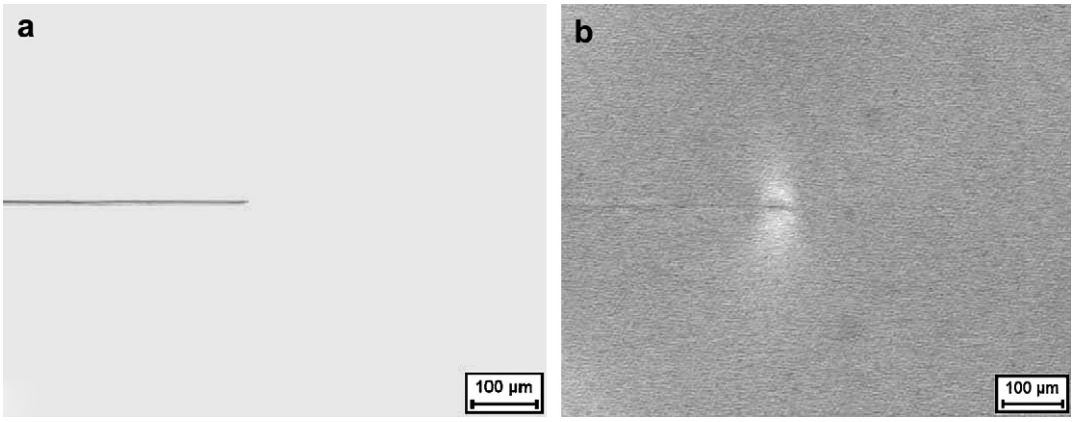


**Fig. 11.** Transmitted light optical micrographs of a section with 30–40 μm in thickness taken at the sub-critically propagated crack in DDS-cured epoxy/nanosilica system: (a) under bright field and (b) under crossed polars.

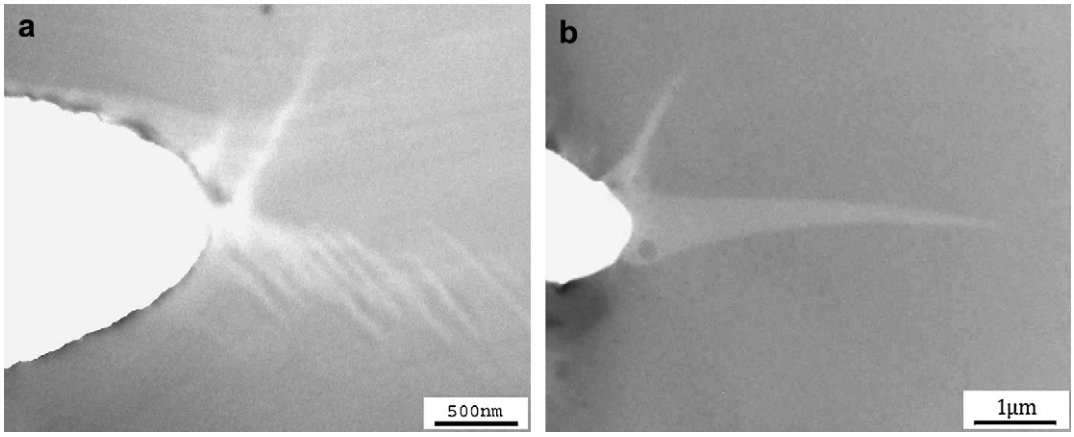


**Fig. 12.** TEM micrographs of a propagated crack tip in neat epoxy cured by J230: (a) without loading and (b) loaded with 80% of the critical load.

figures indicate that the nanoparticle number per area in this zone is much lower than the surrounding matrix; these particles neither cavitate nor debond. The formation of this zone can be described as follows: upon loading, a high stress concentration occurred at the crack tip, which caused a local dilatation. The silica nanoparticles have strong interface with and are much stronger than the matrix; on the other hand, the nanoparticles have significant interface area than their peer micron-size particles. Otherwise, internal cavitation or interface debonding would have been observed. Thus, any deformation of silica nanoparticles is unlikely. Upon loading, stress concentrated around silica nanoparticles and formed stress fields due to the difference of Young's modulus and Poisson ratio between epoxy and silica. The stress fields overlapped each other and highly constrained the development of the local dilatation. Upon further

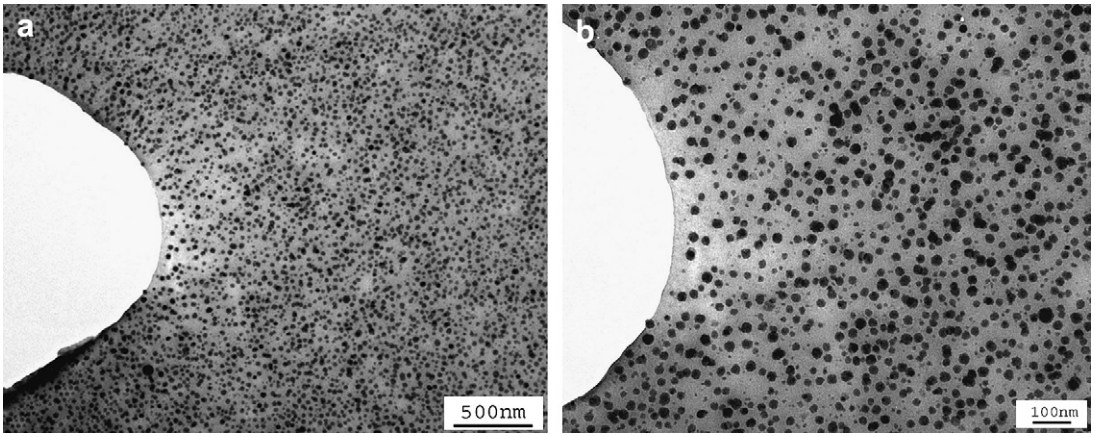


**Fig. 13.** TEM micrographs of a propagated crack tip without loading in J230-cured nanocomposite (20 wt%).

tensile loading, therefore, the dilatation zone thinly propagated along a planar direction perpendicular to the tensile loading. The formation and development of this zone relieved the geometric and stress constraints. Thus, the nanosilica particle number per area in the zone is lower than the surrounding area. Under the sub-critical loading, the zone was able to propagate nearly 1 mm. The further away from the crack tip the micrograph location is, the less obvious the zone is. At 800 μm away (Fig. 19), the particle number per area in the zone is similar to the surrounding area; at 1 mm away (Fig. 20), the zone is almost indiscernible.

In Fig. 14b, an irregular ellipse void of 200–300 nm in diameter was found ahead of the sub-critically propagated crack tip; the void irregularity may be caused by silica nanoparticles. As discussed in the forgoing, the nanosilica-induced stress fields highly constrained the development of the local dilatation and may prevent the void growth. In Fig. 14c, a nanovoid was observed close to the void, near which no nanoparticles were found. This indicates the nanovoid originated from the matrix, instead of the silica nanoparticles.

The silica nanoparticles have strong interface with and are much stronger than the matrix, so nanovoids unlikely initiate from the nanoparticles or the interface between the particle and the matrix. Otherwise internal cavitation or interface debonding would have been observed. Upon loading, stress concentrated around silica

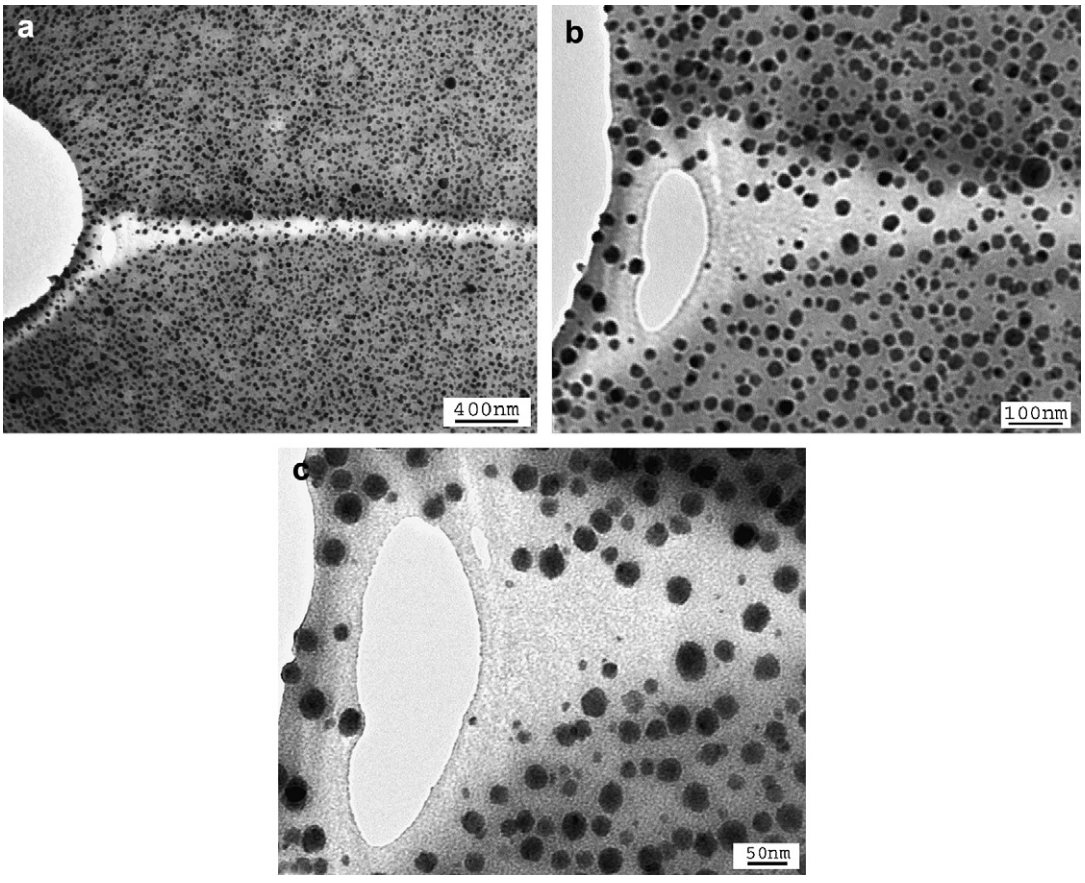


**Fig. 14.** TEM micrographs of a sub-critically propagated crack tip in J230-cured nanocomposite (20 wt%).

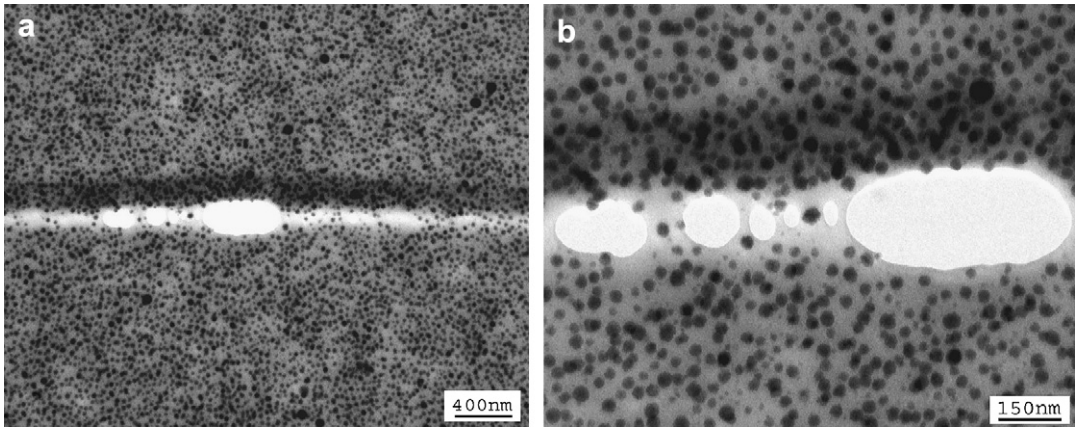


**Fig. 15.** TEM micrographs taken 10 μm away from the sub-critically propagated crack tip in J230-cured nanocomposite (20 wt%).

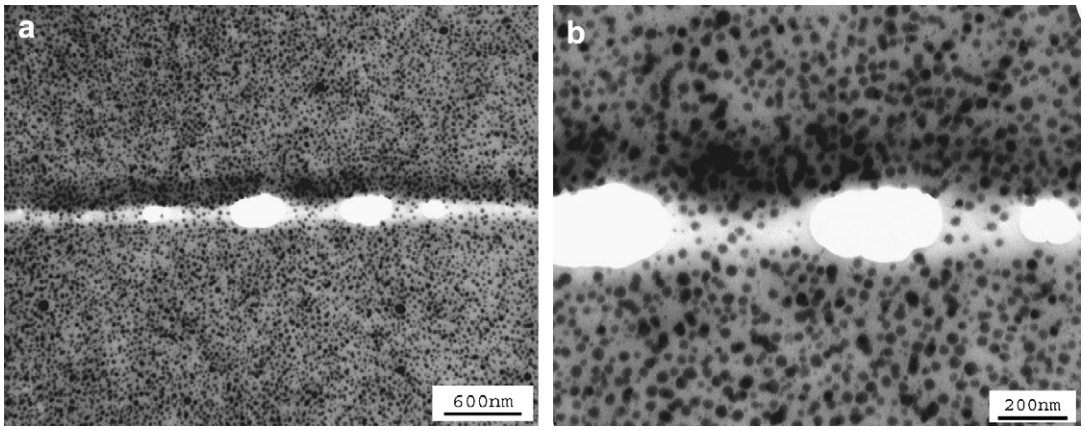


**Fig. 16.** TEM micrographs taken 50 μm away from the sub-critically propagated crack tip in J230-cured nanocomposite (20 wt%).

nanoparticles and formed stress fields due to the difference of Young's modulus and Poisson ratio between epoxy and silica. The stress fields overlapped each other and highly constrained the development of the local dilatation. As loading intensified the nanosilica-induced stress fields, fracture in the form of nanovoids initiated from the overlapped area of these fields. This explains why nanovoids originated from the matrix.

Under continuous loading, these nanovoids would grow as long as formed. On the other hand, the nanosilica-induced stress fields certainly thwarted the void growth, resulting in the void irregularity (Figs. 14c, 15b, 16b and 17b). Once a nanovoid developed, the surrounding material was relieved from further dilatation.

The controlling parameter for the dilatation development and void growth may be the hydrostatic stress in the zone. The closer to the tip the void, the higher degree the hydrostatic stress is, corresponding to a higher degree of the zone development and void growth. At 10 μm away from the crack tip (Fig. 15b), a thin dilatation zone and a number of voids, ranging from 50 to

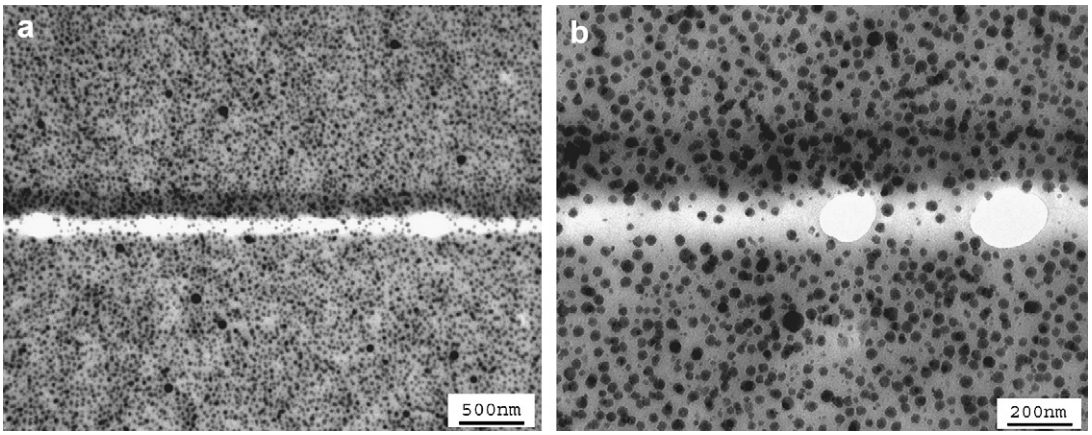


**Fig. 17.** TEM micrographs taken 200 μm away from the sub-critically propagated crack tip in J230-cured nanocomposite (20 wt%).

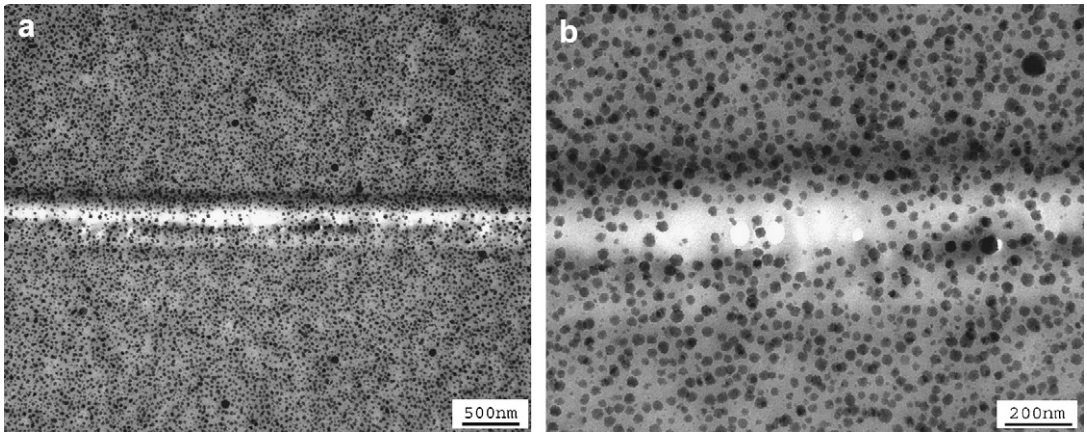


**Fig. 18.** TEM micrographs taken 500 μm away from the sub-critically propagated crack tip in J230-cured nanocomposite (20 wt%).

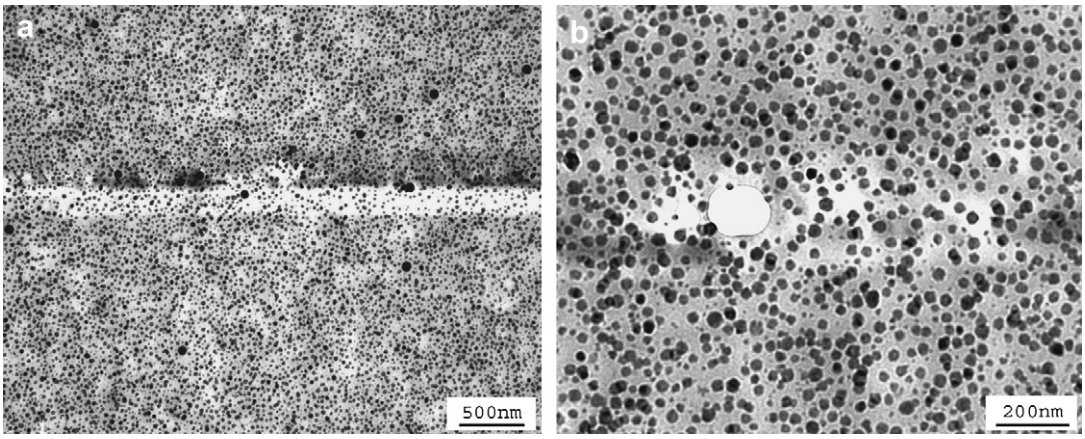


**Fig. 19.** TEM micrographs taken 800 μm away from the sub-critically propagated crack tip in J230-cured nanocomposite (20 wt%).

500 nm in diameter, were found in the zone. These voids developed along the zone propagation plane are perpendicular to the loading direction for two reasons. One is that the lower nanosilica particle number per area leads to less intensity of the nanosilica-induced stress fields than the surrounding area; the other is that the hydrostatic stress in this zone decreases further away from the crack tip. At 50 μm away from the crack tip (Fig. 16b), both the amount and the size of the voids decrease. Further away from the tip as shown in Figs. 17b, 18b and 19b, similar trend is found until the zone is not discernable at 1 mm away (Fig. 20).

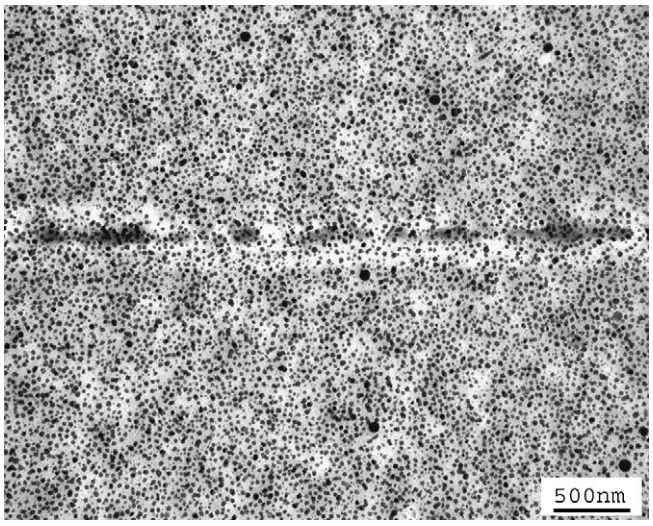


**Fig. 20.** TEM micrographs taken 1000 μm away from the sub-critically propagated crack tip in J230-cured nanocomposite (20 wt%).

The toughening mechanisms in J230-cured nanocomposite, which are schematically shown in Fig. 21 can be described as follows: (1) when subjected to loading, a high stress concentration occurs at the naturally sharp crack tip, which induces local dilatation. As the silica nanoparticles are much stronger than and have a strong interface with the matrix, particle deformation, internal cavitation and interface debonding would not occur under loading. Instead, stress concentrates in the surrounding area of silica nanoparticles and stress fields are formed due to the difference of Young's modulus and Poisson ratio between epoxy and silica. The stress fields highly constrain the development of the local dilatation. (2) With continued loading, the local dilatation develops and extends into the matrix. As the dilatation is highly constrained by the nanosilica-induced stress fields, the dilatation develops in the plane of the crack propagation trajectory, which is perpendicular to the tensile direction. As a result, an extremely thin dilatation zone of ~100 nm in thickness with lower nanoparticle number per area is formed. The formation of this zone relieves the geometric and stress constraints. On the other hand, the loading

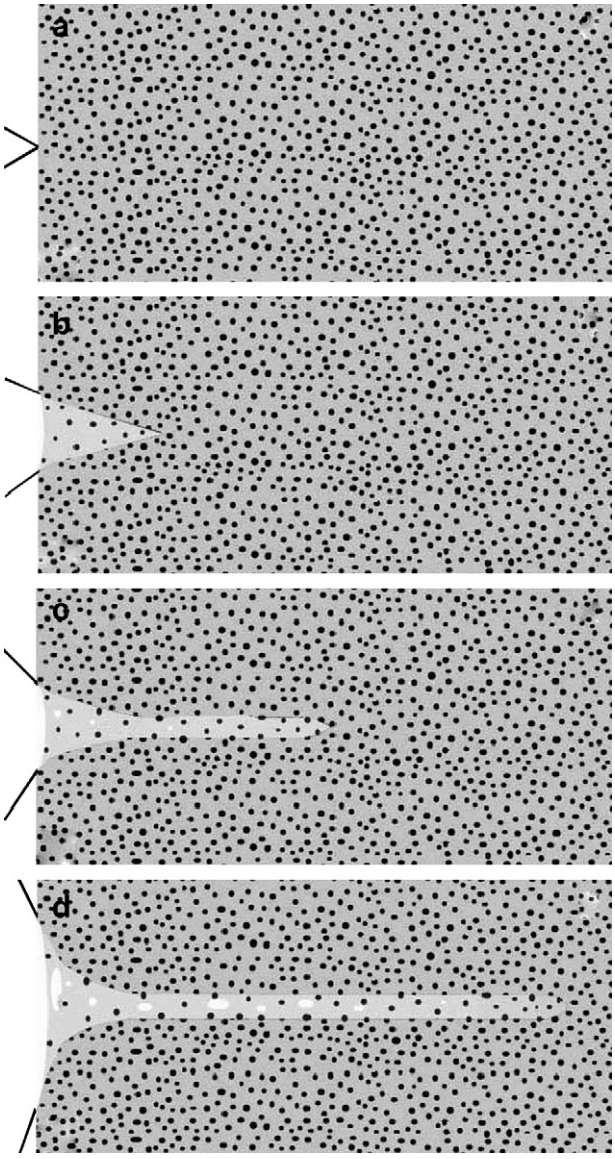


**Fig. 21.** Illustration of the dilatation initiation and propagation processes in the epoxy/silica nanocomposites cured by J230: (a) the initial starter crack; (b) local dilatation zone constrained by silica nanoparticles; (c) the formation of the thin dilatation zone and nanovoids and (d) propagation of the zone and void growth.

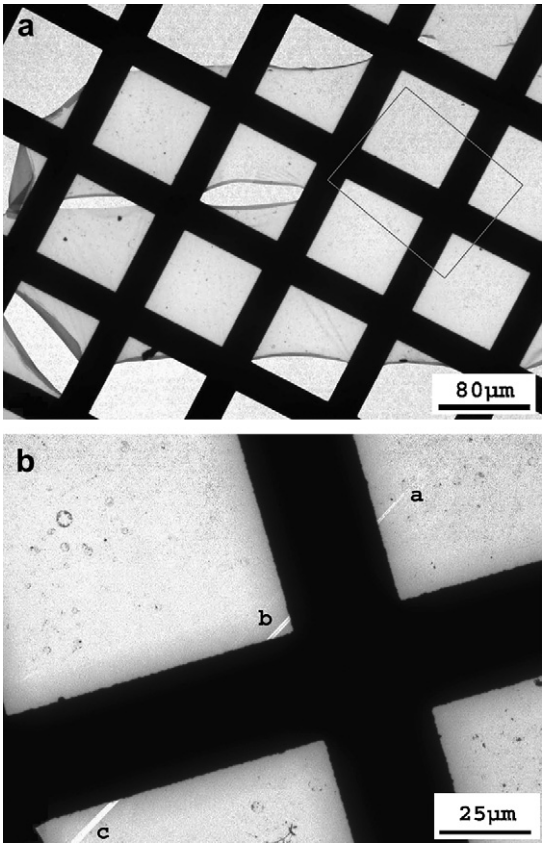


**Fig. 22.** TEM micrographs from sub-critically propagated crack tip in J230-cured nanocomposite (10 wt%).

increases the intensity of the nanosilica-induced stress fields so that these fields overlap each other. As a result, nanovoids initiate from the overlapped stress fields of the silica nanoparticles (Figs. 14c, 15b and 18c). (3) Upon further loading, the dilatation zone develops and extends into the matrix in the direction of the crack propagation trajectory. On the other hand, the nanosilica-induced stress fields thwart the void growth, as shown in Figs. 14c, 15b, 16b, 17b, 18b and 19b. This helps to release the strain energy. Finally, these voids grow and coalescence into micro-voids and cracks, causing catastrophic fracture.

Kinloch et al. reported that nanoparticle debonding and subsequent plastic void growth were major toughening mechanisms of epoxy/silica nanocomposite [4]. However, the nanoparticle

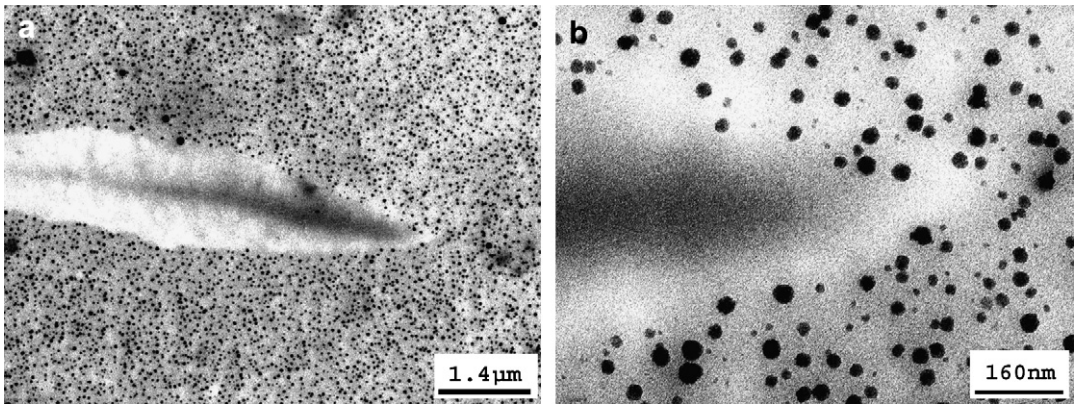


**Fig. 23.** TEM micrographs from location a in Fig. 22b.

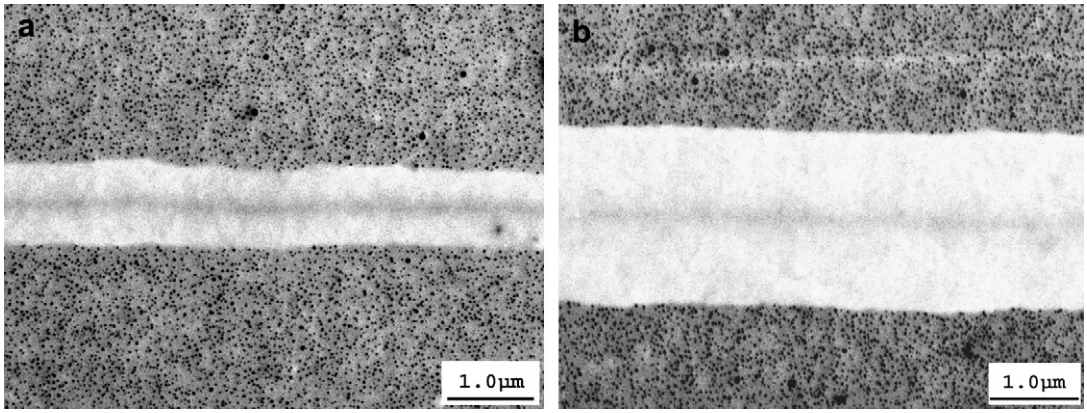


**Fig. 24.** TEM micrographs: (a) from location b in Fig. 22b; (b) from location c in Fig. 22b.

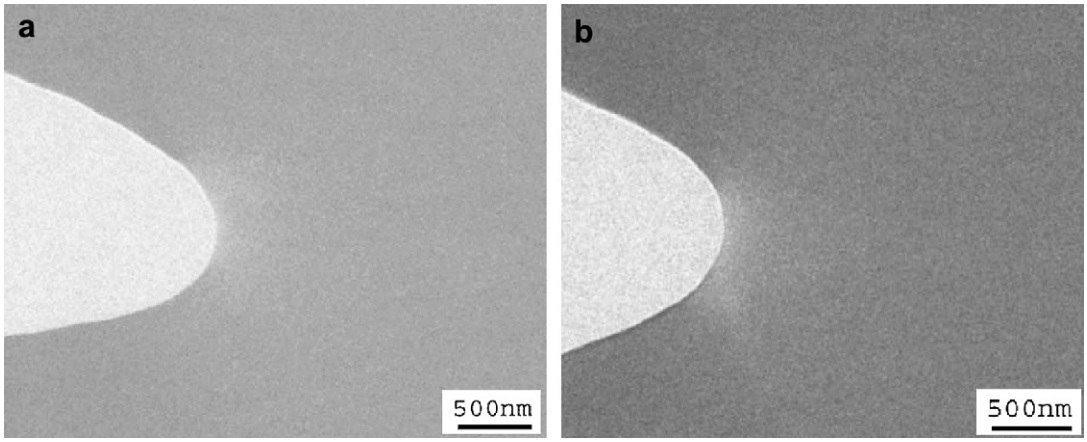


**Fig. 25.** TEM micrographs of a propagated crack tip in DDS-cured neat epoxy: (a) without loading and (b) loaded with 80% of the critical load. The crack propagates from left to right.

debonding was not observed at all in this research. This could be explained by the following reasons: (a) Different hardener used: Kinloch cured epoxy using methylhexahydrophthalic acid anhydride; J230 was used in this research as the hardener. Thus, different hardeners may produce very different interface adhesions. (b) Insufficient identification techniques: scanning electron microscope and atomic force microscope were used in the former research to provide evidence for particle debonding. Both microscopes provide only surface information. In contrast, TEM micrographs from the vicinity of a sub-critically propagated crack tip provide an on-site quantitative measurement of the fracture information with a function of distance to the crack tip.

Artifacts may be caused by the ultramicrotome diamond knife used for TEM section preparation. If the thin dilatation zone and the nanovoids are artifacts produced by the knife, then the dilatation zone and the voids should have been observed throughout the whole section. In fact the zone and the voids were not found throughout the section. We indeed reproduced the thin dilatation zone and the nanovoids with another diamond knife.

To investigate the correlation between the dilatation dimension and the nanoparticle fraction, a sub-critically propagated crack of J230-cured nanocomposite containing 10 wt% silica nanoparticles was analyzed. Fig. 22a contains a low magnification TEM micrograph of the nanocomposite. The vicinity in front of the sub-critically propagated crack tip, included by a rectangle in Fig. 22a, is magnified in b. A thin dilatation zone of ~250 μm in length can be clearly identified. Three locations a–c of the zone are magnified in Figs. 23, 24a and b, respectively. No particle debonding is found throughout all micrographs. The front of the dilatation zone (location a) is shown in Fig. 23. The zone at location b shows a thickness of ~900 nm in Fig. 24a, while it increases to ~1500 nm in Fig. 24b. The following comparisons were made for the forgoing two nanocomposites cured by J230: (a) with increasing the nanoparticle fraction from 10 to 20 wt%, the dilatation zone thickness reduces while the zone length increases significantly; (b) silica

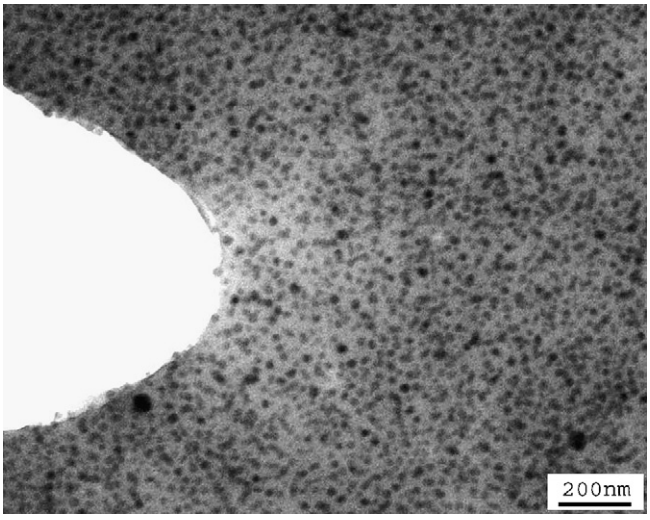


**Fig. 26.** TEM micrographs of a propagated crack tip without loading in DDS-cured nanocomposite (20 wt%).

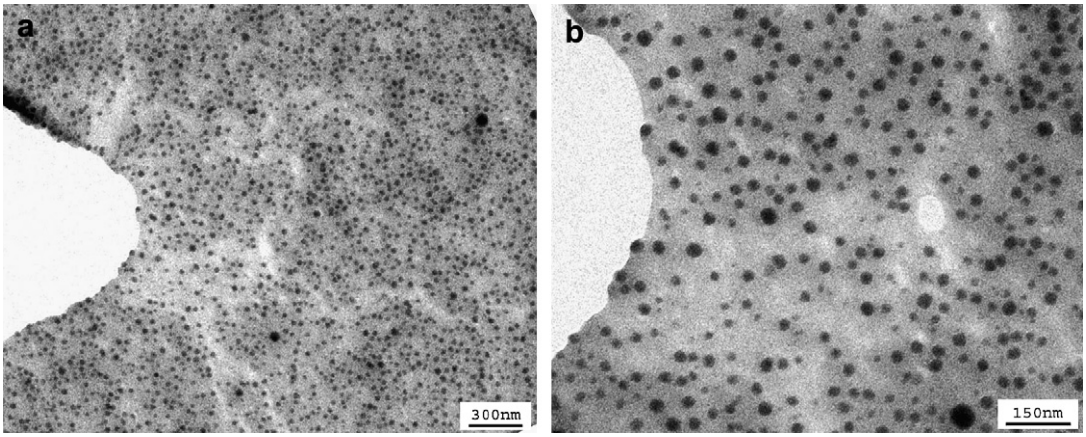


**Fig. 27.** TEM micrographs of a sub-critically propagated crack tip in DDS-cured nanocomposite (20 wt%).

nanoparticles and nanovoids are observed in the dilatation zone of the 20 wt% nanocomposite, while neither nanoparticles nor nanovoids can be found for the 10 wt% nanocomposite.

Fig. 25a includes a propagated crack tip of DDS-cured neat epoxy without loading; no trace of deformation is found. Upon a sub-critical loading, in Fig. 25b, little amount of deformation is observed at the crack tip; this means that a naturally sharp crack tip of neat DDS-cured epoxy is of little capability to create a local dilatation while loaded, in contrast to the neat J230-cured epoxy (Fig. 12b).

TEM micrograph from the vicinity in front of a propagated crack tip of DDS-cured nanocomposite containing 20 wt% silica without loading is given in Fig. 26. Different to the neat epoxy (Fig. 25a), a small local dilatation was found, in which the nanosilica particle number per area is smaller than that in the other areas.

Fig. 27 shows TEM micrographs from the vicinity in front of the sub-critically propagated crack tip of DDS-cured nanocomposite with a sub-critical loading. Local dilatation is found in Fig. 27a; a nanovoid can be identified at a higher magnification (Fig. 27b). Different to J230-cured nanocomposites (Figs. 14–20), we have not observed a thin dilatation zone and nanovoid. This is due to the hardeners used. J230 is a flexible, long chain molecule, providing flexibility to epoxy; DDS is a stiff, short chain molecule, offering higher modulus and less molecular flexibility to epoxy. Therefore, neither thin dilatation nor nanovoids in the DDS system are able to occur, leading to a moderately improved toughness (Fig. 8).

Given the evidence shown in Fig. 8, the formation of local dilatation of the DDS-cured nanocomposite can similarly reduce the stress concentration induced by flaws during tensile testing, and this explains why the silica nanoparticles reduced the standard deviation of the tensile strength.

## 4. Conclusions

New toughening mechanisms for inorganic nanoparticle-toughened epoxy were identified using a new method in this paper, which may provide important fracture information to other inorganic nanoparticle-toughened systems.

The 20–30 nm silica nanoparticles with strong interface were evenly dispersed in the matrix. These nanoparticles increased tensile strength and diminished the effect of flaws on the mechanical performance of brittle epoxy; the significantly improved Young's modulus may be independent of the hardener used; although the nanoparticles made crack propagation more unstable, the energy release rate was enhanced by 274% for J230-cured epoxy and by 81% for the other system.

The initiation and development of a thin dilatation zone and nanovoids are the dominant toughening mechanisms for the J230-cured system containing 20 wt% silica nanoparticles. These nanoparticles are much stronger than and have a strong interface with the matrix; on the other hand, the nanoparticles have significant interface area in comparison with their peer micron-sized particles. Therefore, particle deformation, internal cavitation and interface debonding would not occur under sub-critical loading. Stress concentrated in the surrounding area of silica nanoparticles and formed stress fields due to the difference of Young's modulus and Poisson ratio between epoxy and silica. The stress fields highly constrained the development of the local dilatation. The loading increased the intensity of the nanosilica-induced stress fields so that these fields overlapped each other. As a result, nanovoids initiated and developed from the overlapped area of the stress fields, which in turn thwarted the nanovoid growth. This helped to release the strain energy and alleviate the tension. As the nanoparticle-induced stress fields highly constrained the deformation, a thin dilatation zone of ~100 nm in thickness containing less nanoparticles was formed. The formation of this zone relieved the geometric and stress constraints. For 10 wt% silica nanoparticle-toughened epoxy, a different thin dilatation zone was found, as it contains neither silica nanoparticle nor nanovoid. This zone is thicker and shorter than that of the 20 wt% nanoparticle-toughened epoxy.

Regarding the DDS-cured nanocomposites, much lower degree of dilatation and nanovoid formation were found, corresponding to the moderately improved toughness.

## Acknowledgments

JM thanks the Australian Research Council for the award of an Australian Postdoctoral Fellowship, tenable at the University of South Australia. The authors thank Prof. Gordon J. Williams and Yiu-Wing Mai for useful suggestions. Mr. J. Terlet and Dr. P. Self at Adelaide Microscopy have kindly provided access and technical support to its facilities.

## References

[1] Ray SS, Okamoto M. Progress in Polymer Science 2003;28:1539.
[2] Rosso P, Ye L, Friedrich K, Sprenger S. Journal of Applied Polymer Science 2006; 101:1235.
[3] Zhang H, Zhang Z, Friedrich K, Eger C. Acta Materialia 2006;54:1833.
[4] Johnsen BB, Kinloch AJ, Mohammed RD, Taylor AC, Sprenger S. Polymer 2006; 48:530.
[5] Ragosta G, Abbate M, Musto P, Scarinzi G, Mascia L. Polymer 2005;46: 10506–16.
[6] Ma J, Yu ZZ, Zhang QX, Xie XL, Mai YW, Luck I. Chemistry of Materials 2004; 16:757.
[7] Ma J, Xu J, Ren JH, Yu ZZ, Mai YW. Polymer 2003;44:4619.
[8] Hanse Chemie. Patent application. WO 02/083776 A1; 2002.
[9] Kang S, Hong S, Choe C, Kim J. Polymer 2001;42:879.

[10] Sue HJ, Yee AF. Journal of Materials Science 1993;28:2975.
[11] Ma J, Qi Q, Bayley J, Du XS, Mo SM, Zhang LQ. Polymer Testing 2007;26:445.
[12] Holik AS, Kambrour RRK, Hobbs SY, Fink DG. Microstructural Science 1979;7:357.
[13] Ma J, Yu ZZ, Kuan SC, Mai YW. Macromolecular Rapid Communications 2005; 26:830.
[14] Ma J, Xiang P, Mai YW, Zhang LQ. Macromolecular Rapid Communications 2004;25:1692.
[15] Ma J, Shi LH, Xu J. Journal of Applied Polymer Science 2002;86:3708.
[16] Ma J, Xu J, Zhu YJ, Zhang LQ. Polymer 2002;43:937.
[17] Chern YC, Tseng SM, Hsieh KH. Journal of Applied Polymer Science 1999;74: 328.
[18] Barone L, Carciotto S, Cicala G, Recca A. Polymer Engineering and Science 2006;46:1576.
[19] Pascoe KJ. An introduction to the properties of engineering materials. 3rd ed. London: Van Nostrand Reinhold; 1978.
[20] Isik I, Yilmazer U, Bayram G. Polymer 2003;44:6371.